Prototype surface contamination monitor with positional sensitivity

Master's thesis, 9.12.2022

Author:

Oskar Çelik

Supervisors:

Panu Rahkila
Paul Greenlees
Teemu Siiskonen (STUK)

UNIVERSITY OF JYVÄSKYLÄ
DEPARTMENT OF PHYSICS

Tiivistelmä

Çelik, Oskar
Prototyyppi paikkaherästä pintakontaminaatiomittarista
Pro gradu -tutkielma
Fysiikan laitos, Jyväskylän yliopisto, 2021, 48 sivua

Tässä työssä rakennettiin prototyyppi pintakontaminaatiomittarista, joka kykeni erottamaan alfa- ja beetasäteilyn toisistaan ja samanaikaisesti mittaamaan kyseisten säteilylähteiden paikan. Motivaationa tälle työlle toimi tarve kehittää tekniikkaa, joka helpottaisi aktiivisuuskatteen paikkaherkkää määrittämistä pintakontaminaation mittaamisessa. Erottelukyky alfa- ja beetasäteilyn välillä saavutettiin asettamalla kerros sinkkisulfidia polyvinyylitolueenista koostuvan tuikemuovin päälle, mittaamalla emittoitunut valo piivalomonistimella, ja erottelemalla eri signaalit pulssimuotojensa perusteella. Neliönmallisen detektorin paikkaherkkyys x-suunnassa saatiin aikaan mittaamalla vaimentuneiden pulssien korkeuksien suhteita, kun tuikepulssi vaimeni paikan funktiona edetessään tuikemuovissa. Paikkainformaatio y-suunnassa saatiin sen perusteella, mistä tuike-elementistä signaali havaittiin. Rakennetun prototyypin ilmaisinala oli $10\,\mathrm{cm} \times 10\,\mathrm{cm}$. Alfa- ja beetasäteilyn erottelu toteutettiin onnistuneesti ja laitteen paikkaresoluutioksi saatiin karkeasti $1\,\mathrm{cm}^2$.

Avainsanat: säteily, kontaminaatio, detektori, valomonistin

Abstract

Çelik, Oskar
Prototype surface contamination monitor with positional sensitivity
Master's thesis
Department of Physics, University of Jyväskylä, 2021, 48 pages.

A prototype contamination monitor was built, which had the ability to separately detect alpha and beta radiation and the ability to simultaniously measure the position of the source of radiation. The motivation behind this work was the need to advance techniques towards locally quantifying surface activity when measuring radioactive surface contamination. The discrimination between alpha and beta radiation was achieved by layering zinc sulphide on a polyvinyltoluene plastic scintillator, measuring the yielded light with a silicon photomultiplier, and using pulse shape discrimination to analyze the two types of signals. Positional sensitivity in the x-direction on the square-shaped detector was achieved by measuring the ratio of pulse heights of attenuated signals, as the pulse height of a scintillation event was a function of position in the plastic scintillator. Positional information in the y-direction was based on which scintillator element the signal was detected from. The size of the detector area was $10\,\mathrm{cm} \times 10\,\mathrm{cm}$ in the finished prototype. The discrimination between alpha radiation and beta radiation was succesful, and a positional accuracy of roughly $1\,\mathrm{cm}^2$ was achieved.

Keywords: radiation, contamination, detector, photomultiplier

Contents

1 Introduction

When working with radioactive materials, especially unsealed radioactive sources, there exists the possibility of contamination. Radioactive contamination is harmful to a persons health, if contaminants are ingested or come in contact with one's skin. To check for radioactive contamination, one needs to measure the surfaces of the working area with a radiation detector suitable for measuring surface contamination. [1, 2]

A typical type of contamination monitor, some of which are presented in Reference [1], is either a Geiger-Müller tube or a scintillator-based detector, which provide qualitative information to the user, such as the type of radiation being detected (i.e. alpha, beta or gamma radiation), and some quantitative information, such as the count rate. The scintillator based contamination monitors often utilize a single photomultiplier to convert the light pulse yielded in the scintillator into an electrical signal, and thus they effectively only indicate whether radioactivity is or is not present. Photomultiplier tubes, while effective at doing the job they are designed for, have the downside of being rather big and they require high operational voltages, of the order of 1 kV [3, 4]. Photodiodes, which are relatively small and require much smaller operational voltages, could be more suitable for compact applications, such as handheld devices. [3]

If a contamination monitor only indicates whether there is contamination on the surface or not, it gives no information about how the contamination is distributed within the measurement area. Regulations by the Finnish Radiation and Nuclear Safety Authority (STUK) require that radioactive contamination on surfaces is quantified to monitor that the levels of contamination are not dangerously high [5]. Currently, to effectively quantify low level contamination, one would have to take a smear sample of the contaminated area and do additional measurements to determine the surface activity. If there were a measuring device that could determine the surface activity directly and locally, say with a resolution of 1 cm^2, the device would have to be capable of determining where exactly on the measured surface the

radiation is coming from. This kind of *ideal* contamination monitor would be able to; separately detect alpha, beta and gamma radiations; measure the energy of the detected gamma rays for nuclide identification; have high positional accuracy within the measurement area, and automatically calculate the activity per surface area of the contamination.

This thesis will cover the process of developing and building a prototype contamination monitor. The purpose of this work is to test the simultaneous implementation of positional sensitivity within the measurement area and discrimination between alpha and beta radiation. All of the necessary theoretical background will be introduced for the benefit of the reader.

2 Theoretical background

2.1 Interaction of ionizing radiation with matter

2.1.1 Gamma rays and x-rays

There are a variety of ways in which high energy photons, *i.e.* gamma rays and x-rays can interact with matter. One of them is the *photoelectric effect*, where a photon is fully absorbed by an atom, while one of the orbital electrons is ejected. Another is the *Compton scattering effect*, in which a photon scatters from a loosely bound electron by giving off some of its energy and changing direction in the interaction. The electron gains the energy lost by the photon as kinetic energy, and it is ejected from the atom. A third possible phenomenon is *pair production*, where a high energy photon interacts with the electric field of an atom's nucleus, and creates an electron-positron pair. The probabilities these interactions occurring depend on the energy of the incident photon and the atomic number of the absorber. Figure 1 presents the regions of energy and absorber mass number, in which each interaction mode is most likely to occur. [3]

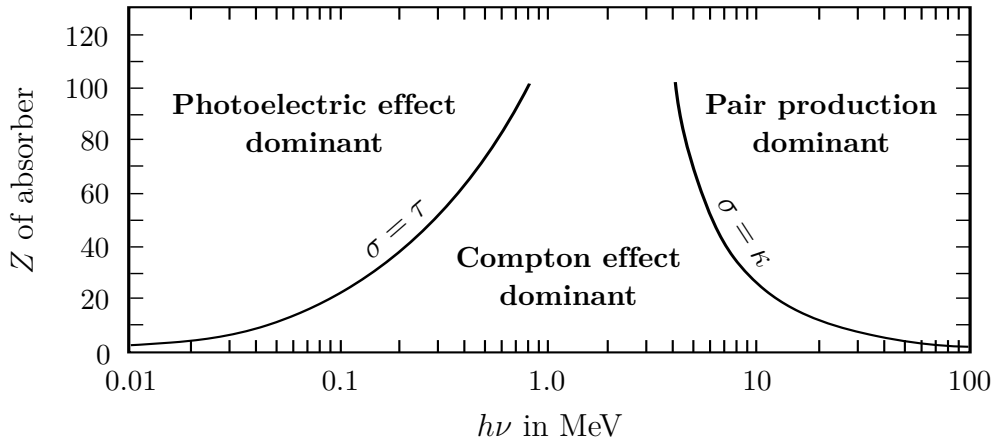

Figure 1. A graph showing when each mechanism of interaction for a high energy photon is most probable. The lines represent when their respective partial attenuation coefficients σ, τ and κ are equal. Figure recreated from Reference [6].

The photoelectric effect is a phenomenon, in which a photon is absorbed by an atom, resulting in the ejection of one of the orbital electrons from one of the innermost electron shells. The effect can only happen when the photon is interacting with the atom in its entirety, as it cannot be fully absorbed by a free electron. An illustration of the photoelectric effect is presented in Figure 2. [3]

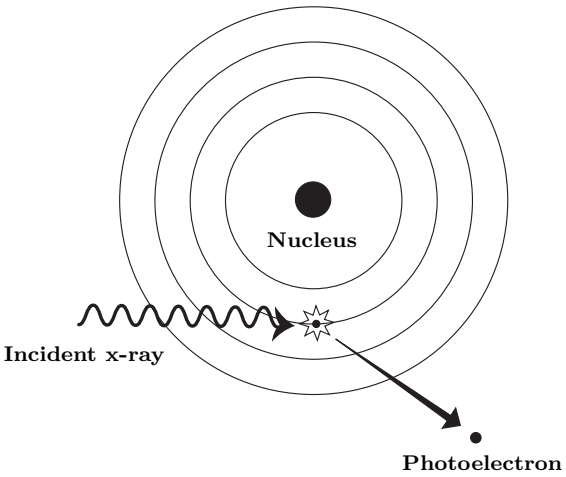

Figure 2. The photoelectric effect. An x-ray photon is absorbed by an atom, which causes an electron to be ejected, leaving the atom ionized and excited. Figure obtained from Reference [7].

The full energy of the photon is lost in the interaction; a portion of the energy is consumed by the ionization process, while the residual energy is gained by the ejected *photoelectron* as kinetic energy. The kinetic energy of the photoelectron is thus

$$E_e = h\nu - E_b, \tag{1}$$

where $h\nu$ is the energy of the absorbed photon, with h being Planck's constant and ν being the photon frequency, and E_b is the binding energy of the electron. The ejected electron creates a vacancy in the orbital, which leaves the atom in an excited state. This is followed by an outer shell electron filling the vacancy, which de-excites the atom by emitting an x-ray photon with an energy characteristic to the particular transition between the energy states. The de-excitation can also occur by the emission of another bound electron known as an *Auger electron*. The emitted characteristic x-rays are most often reabsorbed close to the site of emission through another photoelectric absorption, by electrons with smaller ionization energy. [3]

Compton scattering, also known as the Compton effect, occurs when a high energy photon scatters off of a free electron or a loosely bound electron. The electron is effectively free when the binding energy is significantly less than the energy of the incident photon. In this interaction, the incident photon loses some of its energy and changes the direction of propagation. The energy lost by the photon is transferred over to the *recoil electron* or *Compton electron* as kinetic energy. An illustration of Compton scattering is presented in Figure 3. [3, 8]

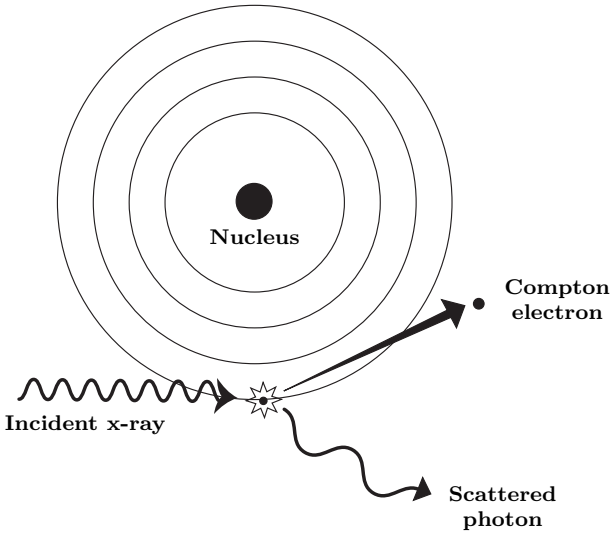

Figure 3. The Compton effect. The incident photon scatters off of an electron that is weakly bound to an atom. The photon changes its direction of propagation, and transfers some of its energy to the recoil electron. Figure obtained from Reference [7].

The energy of the scattered photon along with its relation to the scattering angle can be written as

$$h\nu' = h\nu \left[1 + \frac{h\nu}{m_e c^2}\left(1 - \cos\theta\right)\right]^{-1}, \tag{2}$$

where hv is the energy of the incident photon, m_e is the rest mass of the recoil electron, c is the speed of light and θ is the photon scattering angle. The higher the scattering angle, the more energy is transferred to the recoil electron. In the extreme case where a photon is scattered back at an angle of 180°, it still retains some of its energy, since a photon cannot be fully absorbed by a free electron, because the simultaneous conservation of energy and momentum would not be possible. [3]

Pair production occurs when a high energy photon interacts with the electric field of an atom's nucleus, which causes the photon to disappear and creates an electron-positron pair. An illustration of this effect is presented in Figure 4. [3]

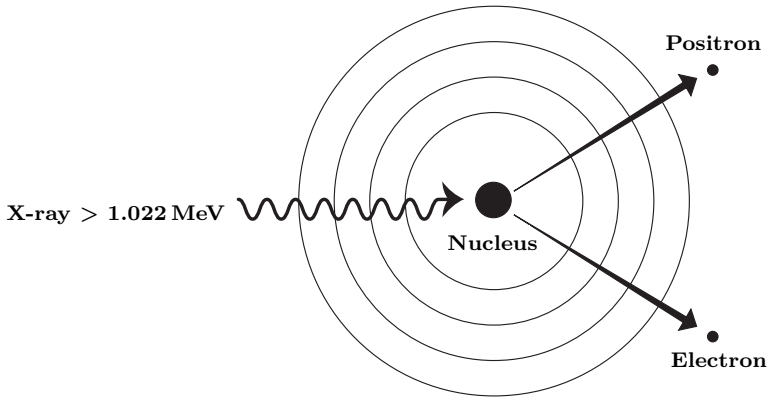

Figure 4. A high energy photon interacting with the electric field of a nucleus. The photon disappears and its energy is converted in to the mass of the electron-positron pair and into kinetic energy of the two particles. Figure obtained from Reference [7].

Pair production is energetically possible only when the energy of the photon is above 1.022 MeV, which is the combined rest energy of the electron-positron pair. Any residual energy that the photon has beyond this energy limit, is shared by the electron and the positron as kinetic energy. At photon energies slightly over 1.022 MeV, pair production, though possible, is very improbable. The effect has a higher probability of occurring, when the energy of the photon is in the several MeV range. Figure 1 shows the photon energies at which pair production becomes the most likely interaction mechanism. The total kinetic energy of the electron-positron pair is

$$E_k^{tot} = E_k^{e^+} + E_k^{e^-} = h\nu - 2m_e c^2 = h\nu - 1.022\,\text{MeV}, \tag{3}$$

where $E_k^{e^+}$ and $E_k^{e^-}$ are the respective kinetic energies of the positron and the electron, $h\nu$ is the energy of the photon, and $2m_e c^2$ is the rest mass of the particle pair, which is equal to 1.022 MeV. The electron that is created in the process can go on to ionize and excite other atoms in the medium, while the positron will annihilate with another electron. The annihilation process creates two gamma rays of 511 keV energies, which can again go on to interact with the medium through the aforementioned photon interaction mechanisms in this chapter. [3]

2.1.2 Alpha radiation

Alpha radiation is the result of *alpha decay*, which occurs when a heavy nucleus ejects a ^{4}He nucleus, *i.e.* an alpha particle, due to instability caused by repulsive interactions within the heavy nucleus. The total kinetic energy released comes at the cost of the mass difference between the parent nucleus, the daughter nucleus and the alpha particle. Alpha decay is described by the equation

$$ {}^{A}_{Z}X \rightarrow {}^{A-4}_{Z-2}X'_{N-2} + \alpha, \tag{4} $$

where X and X' refer to the parent and the daughter nuclei.

The kinetic energy of the alpha particle is typically in the 5 MeV range. Alpha particles are emitted monoenergetically, because it is a two body process, in which there is an unambiguous way for the released energy to be divided between the products. Alpha decay is show in Figure 5. [9, 4]

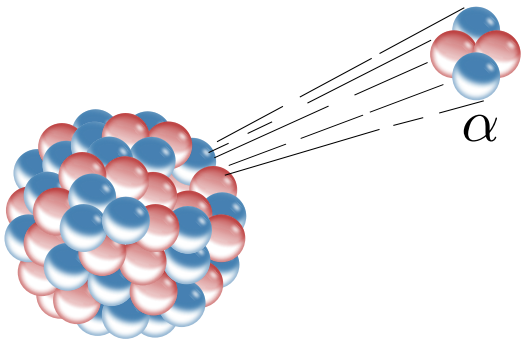

Figure 5. Emission of an alpha particle by a heavy unstable nucleus. The red nucleons represent protons and the blue nucleons represent neutrons. Figure from Reference [10].

Alpha particles deposit energy into a medium primarily through Coulomb interactions between the positively charged alpha particles themselves and the negatively charged atomic electrons in the medium. They can also interact with the nuclei of the absorbing matter, either through Rutherford scattering or through nuclear reactions, but these interactions are rare and do not significantly contribute to the energy deposited to the medium by the incident alpha particle. [3]

Classically, the maximum amount of energy transferred in a collision between an

incident alpha particle and an electron at rest is

$$E_{K_{max}} = 4E_\alpha \frac{m_e}{m_\alpha}, \tag{5}$$

where E_α is the initial kinetic energy of the incident alpha particle, while m_e and m_α are the masses of the electron and the alpha particle, respectively. This is also the energy obtained by the electron in the collision and it is roughly 1/2000 of the initial kinetic energy of the alpha particle. Equation (5) can be derived by writing out the conservations of kinetic energy and momentum for an elastic collision, and solving for the kinetic energy of the electron, while allowing $m_e \ll m_\alpha$. The energy deposited to the electrons through these interactions is usually sufficient to cause excitation and ionization in the absorbing medium. [3]

When an alpha particle passes through a medium, it interacts with many electrons simultaneously and slows down as a result of the energy lost in these interactions. Since the mass of the alpha particle is much greater than the mass of the electron, and because the energy lost in a single interaction is a small fraction of the initial energy, the alpha particle is not significantly deflected from its path. It is because of this, that the path of the alpha particle is evidently a straight line, with the exception of a possible small deflection right before stoppage. Alpha particles thus have a well defined range within a medium, which is illustrated in Figure 6. [3]

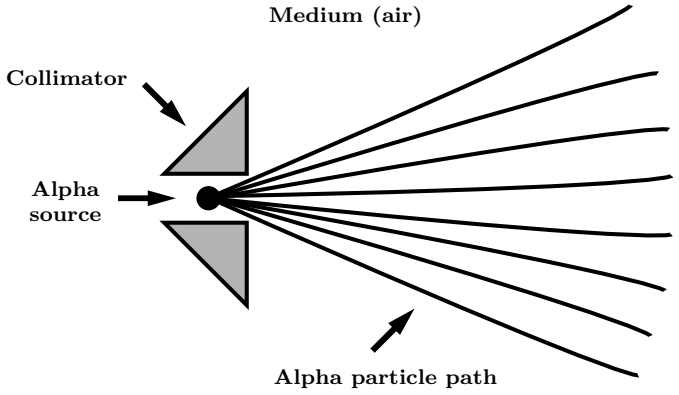

Figure 6. A visual representation of how alpha particles travel through matter. The path of an alpha particle is virtually a straight line, with the exception of small deflection at the end of its path. Figure recreated from Reference [3].

In interactions where the energy transfer is sufficient to ionize atoms in the medium,

the ejected electrons can have enough energy to create ionization paths of their own. These ionization paths caused by secondary electrons are referred to as *delta rays*. The paths of these delta rays are often very short compared to the primary ionization path of the alpha particle, and the secondary ionizations thus occur very close to the primary path. [3]

Stopping power, which can also be referred to as the rate of energy loss per distance, for heavy charged particles is described by the *Bethe formula*, which is written as

$$-\frac{\mathrm{d}E}{\mathrm{d}x} = \frac{4\pi e^4 z^2}{m_e v^2} NB, \tag{6}$$

where

$$B = Z\left[\ln\left(\frac{2m_e v^2}{I}\right) - \ln\left(1 - \frac{v^2}{c^2}\right) - \frac{v^2}{c^2}\right]. \tag{7}$$

The v in Equations (6) and (7) stands for the velocity of the charged particle, ze stands for its charge, Z is the atomic number of the absorber atoms and N is the number density of the absorber atoms (*i.e.* number of atoms in a given volume), while I is an experimentally determined value for the average excitation and ionization energy of a specific absorber material. When v is nonrelativistic, the terms containing c are not significant. The Bethe formula shows that the rate of energy loss increases as the velocity decreases, because of the $1/v^2$ dependency, which dominates over the logarithmic dependency of v^2 in B.

2.1.3 Beta radiation

Beta radiation, which is the result of *beta decay*, is the emission of fast electrons or positrons from the nucleus of an atom. Electrons from beta decay are emitted, when a neutron in an unstable nucleus loses some of its mass and emits a fast electron along with an electron antineutrino. Positrons are conversely emitted, when a proton is converted into a neutron, emitting a positron along with an electron neutrino. These processes are respectively called negative and positive beta decays, and they are described by equations

$$n \rightarrow p + e^- + \bar{v} \tag{8}$$

and

$$p \rightarrow n + e^+ + v, \tag{9}$$

where p and n, refer to a proton and a neutron, e^- and e^+ refer to an electron and a positron, and $\bar{v}$ and v refer to an antineutrino and a neutrino. Orbital electron capture, where a proton in an atom captures an orbital electron and is converted into a neutron, is also a type of beta decay. This results in the emission of a neutrino, but no fast electrons or positrons. An illustration of beta decay is presented in Figure 7.

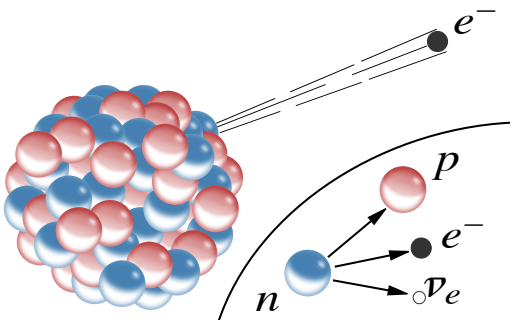

Figure 7. The emission of an electron via negative beta decay. Figure obtained from Reference [10].

The decaying nuclei do not emit these particles monoenergetically, unlike in the case of alpha decay. Beta decay is a three body process, in which there is ambiguity in the way the energy can be distributed between the three particles. Instead of monoenergetic emission, the emitted particles have a distribution of energies. A spectrum of energies of beta particles emitted by a beta active nucleus is presented in Figure 8. [3]

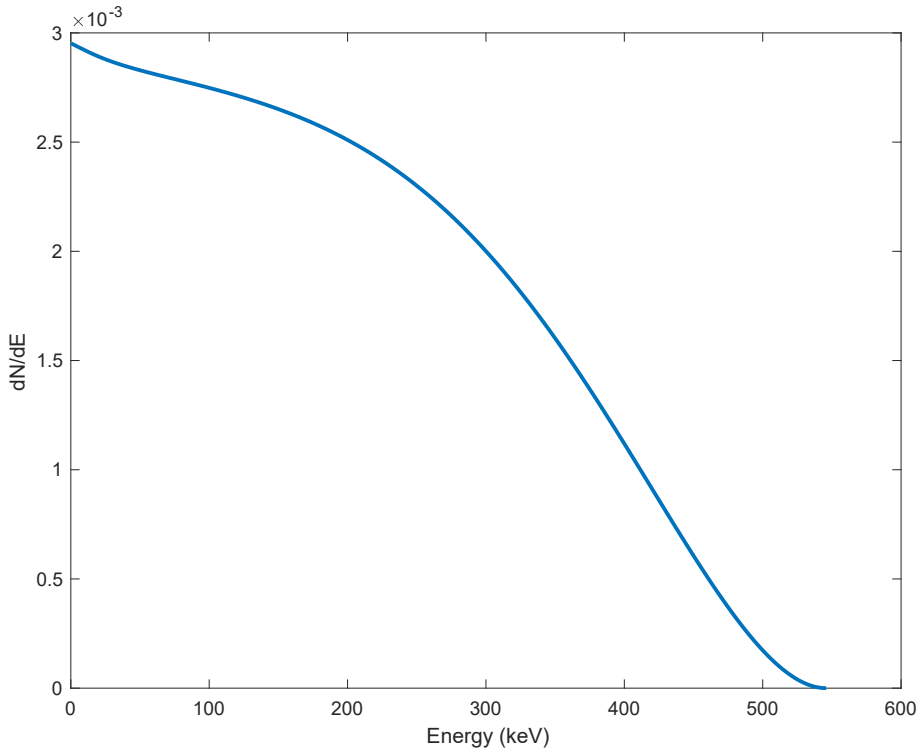

Figure 8. The beta spectrum of ^{90}Sr. Data obtained from Reference [9].

Fast electrons or positrons do not have a well-defined range in a medium like alpha particles do. Figure 9 shows the more complicated path that fast electrons take through a medium. As their mass is equal to that of the bound and free electrons in the medium with which they interact, large changes in direction can occur with every collision. For both electrons and positrons, the Coulomb interactions are the major mechanism for energy loss in an absorber. Whether it be attractive or repulsive forces that slow down the particle, the energy transfer rates for particles of equal mass are approximately the same. In the case of positrons, once they reach the end of their path they annihilate with an electron, releasing two photons of 511 keV energy. [4, 3]

Beta particles lose energy continuously, either from collisions with other electrons of radiative losses of energy. The collisional losses stem from the ionizations and excitations caused by the electron in the absorber material. The rate of energy loss from these collisional interactions is described by an equation similar to the Bethe

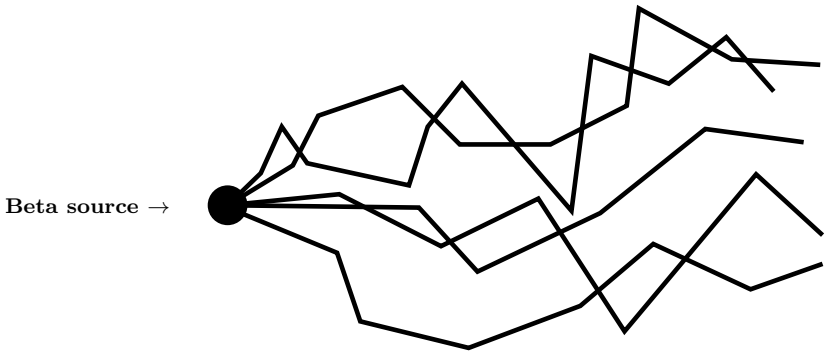

Figure 9. The path of beta particles through a medium.

formula. The collisional rate of energy loss is

$$-\left(\frac{\mathrm{d}E}{\mathrm{d}x}\right)_c = \frac{2\pi e^4 NZ}{m_e v^2}\left[\ln\left(\frac{m_e v^2 E}{2I^2(1-\beta^2)}\right) - \ln 2\left(2\sqrt{1-\beta^2} - 1 + \beta^2\right) + (1+\beta^2) + \frac{1}{8}\left(1-\sqrt{1-\beta^2}\right)^2\right], \tag{10}$$

where $\beta = v/c$, and the remaining symbols are the same as in Equations (6) and (7). The radiative energy loss is caused by the electrons being deflected by Coulomb forces caused by the nuclei of the absorbing material. The radiative loss of energy manifests itself in the form of *Bremsstrahlung*, or braking radiation, which is x-rays being emitted due to these deflections. The equation for the rate of radiative energy loss is

$$-\left(\frac{\mathrm{d}E}{\mathrm{d}x}\right)_r = \frac{NEZ(Z+1)e^4}{137 m_e^2 c^4}\left[4\ln\left(\frac{2E}{m_e c^2}\right) - \frac{4}{3}\right], \tag{11}$$

where the symbols are the same as they are in Equations (6) and (7). The total linear stopping power for electrons is the sum of Equations (10) and (11) as follows,

$$\left(\frac{\mathrm{d}E}{\mathrm{d}x}\right) = \left(\frac{\mathrm{d}E}{\mathrm{d}x}\right)_c + \left(\frac{\mathrm{d}E}{\mathrm{d}x}\right)_r, \tag{12}$$

where the subscript indices c and r refer to collisional and radiative processes respectively. [3]

2.2 Scintillation detectors

2.2.1 Scintillation and scintillating materials

Scintillation is the emission of light caused by a high energy particle passing through a medium. The passing particle excites and ionizes the atoms in the medium and causes fluorescence. The particle causing this phenomenon could be a beta particle, an alpha particle, a proton, a neutron, a heavy ion, or a secondary electron emanating from a photon interaction. Scintillating materials can exist in the form of inorganic alkali-halide crystals, organic plastics or liquids, or other molecules comprising of metalloids and earth alkali metals, for example. [3, 11]

Organic scintillators work *as is*, meaning that the fluorescence is emitted from energy level transitions of individual molecules, so they can emit light in any physical form, whether it be a solid crystal, a solution or vapor. Inorganic scintillators are required to be in crystalline form for them to work as scintillators. [3]

Anthracene, which amongst organic scintillators has one of the highest light yields per energy deposited, exists in crystalline form, but can be mixed with a synthetic polymer such as polyvinyltoluene, to make a plastic scintillator. One benefit of a plastic scintillator is that it can be easily shaped and manipulated into whatever kinds of detector applications. [3] Polyvinyltoluene, or PVT, doped with anthracene is one of the main components used in the production of the prototype described in this thesis.

2.2.2 Photomultipliers

To quantitatively measure scintillation and convert it into an electrical signal, a *photomultiplier* (PM) is needed. Photomultipliers exist in the form of traditional photomultiplier tubes, and nowadays also as semiconductor photodiodes, such as *silicon photomultipliers* (SiPM).

Traditional photomultiplier tubes work by the photoemission of low energy electrons from a photocathode, and then the multiplication of these electrons through a cascade process through several dynodes, with high voltages in between. The whole system is encased in a vacuum tube with a transparent glass window for the light to be detected. A schematic of a photomultiplier tube is shown in Figure 10.

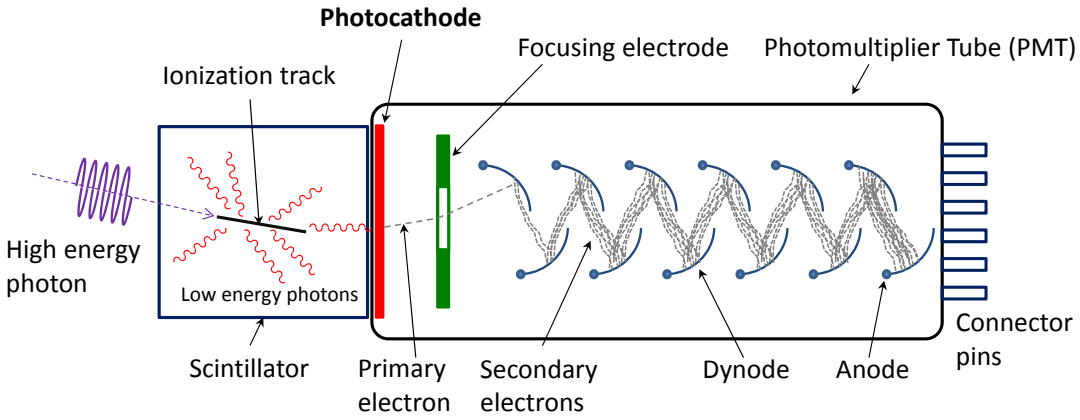

Figure 10. Photomultiplier tube schematic. Low energy photons from a scintillator hit the photocathode, which in turn emits electrons that are accelerated towards the arrangement of dynodes for the signal to be multiplied. Figure from Reference [12].

Photomultiplier tubes are traditionally big and bulky and require high operational voltages, since the voltage difference between dynodes is typically around 100 V, so a 10–dynode tube would require 1 kV of total operational voltage. [3, 4]

Photodiodes also offer the conversion of photons into eletrical signals, but with a handful of benefits when compared to PM tubes. Photodiodes in general have better efficiency, consume less power and are much smaller in size. They also don't require high operational voltages like PM tubes do. One type of photodiode is the silicon photomultiplier, or a SiPM, which is an array of avalanche photodiodes. Silicon photomultipliers are utilized in the apparatus that was built for this thesis work. [3] An example of a silicon photomultiplier is shown in Figure 11.

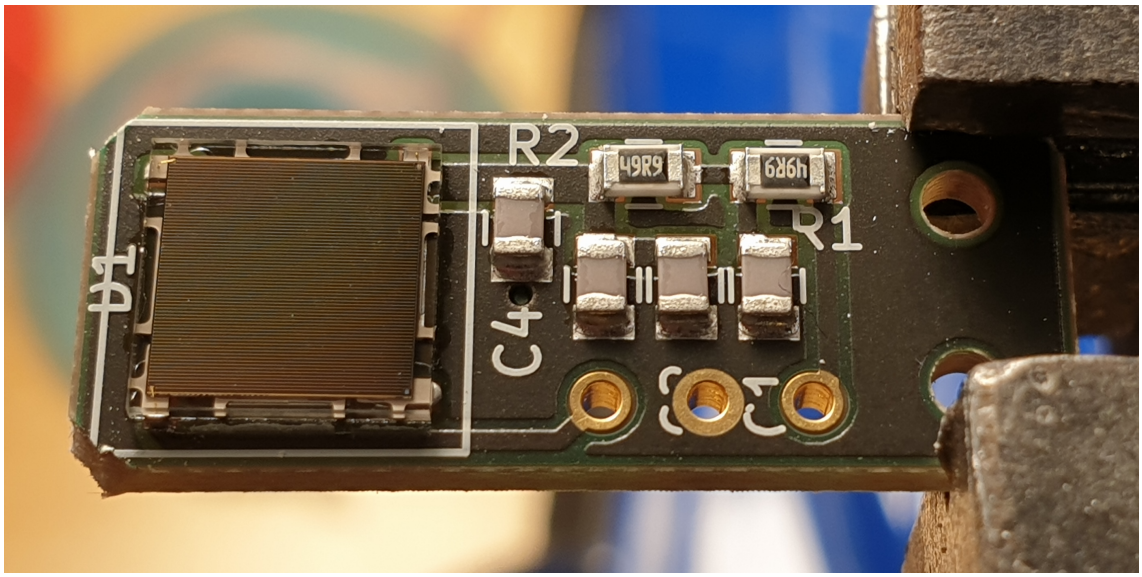

Figure 11. A silicon photomultiplier chip on a printed circuit board.

2.2.3 Detection of radiation

Since scintillating materials fluoresce under ionizing radiation, and photomultipliers can be used to detect light pulses and convert them into electrical signals, these two can be combined to produce an apparatus for electrically detecting ionizing radiation. All one needs to do to build a scintillator-based radiation detector, is to optically couple a piece of scintillating material to a photodiode, or a photomultiplier tube, and then measure the electrical signal with something, for example a digital oscilloscope. In this way, when a high energy particle hits the piece of scintillator, it produces light, which is detected by the photomultiplier, which in turn converts this light into an electrical signal which can be recorded. When assembling such a detector, measures need to be taken in order to ensure isolation from light coming from the surroundings. An example of a simple scintillation detector is presented in Figure 12.

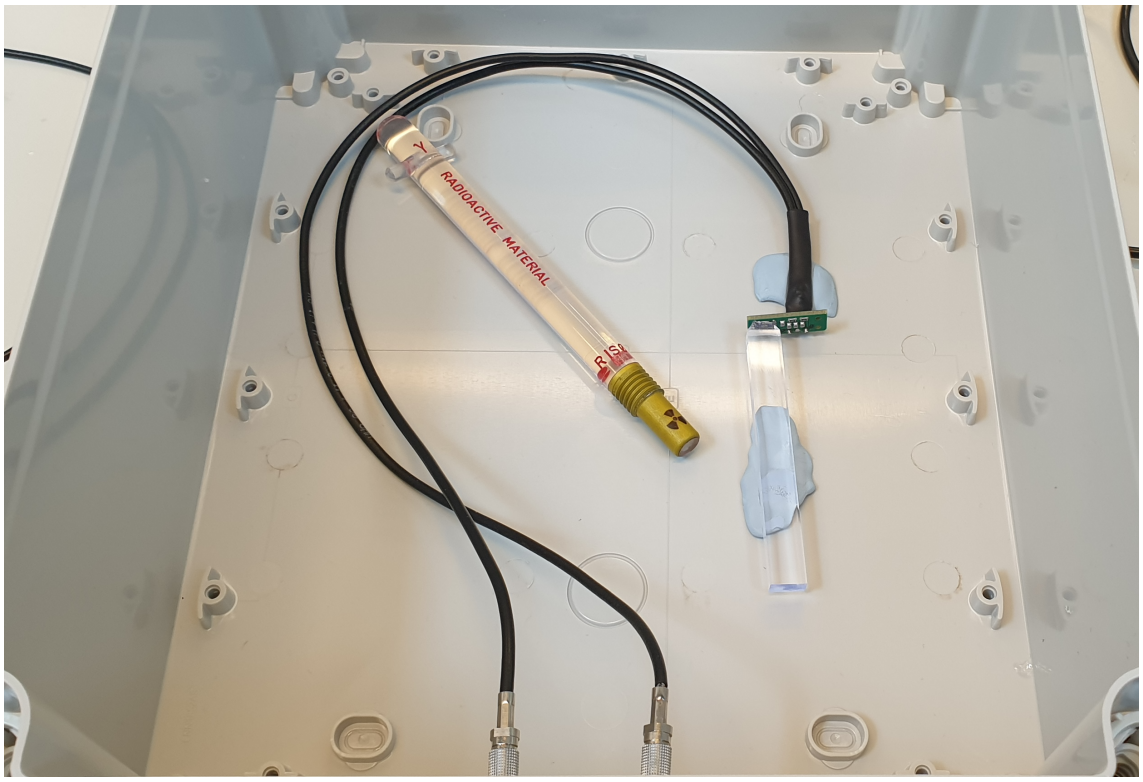

Figure 12. A scintillation detector in its most basic form. A piece of scintillator plastic is coupled to a silicon photomultiplier via a transparent optical grease. A source of radiation is pointed towards the piece of scintillor material to produce a signal. A coaxial cable is connected to a digital oscilloscope for the electrical signal to be measured, while anothed cable delivers the bias voltage required for the photomultipliers operation.

2.3 Radioactive contamination

Whenever radioactive materials are handled, there exists the possibility of contamination. Radioactive contamination can be harmful to a person's health, if it results in radioactive materials to be ingested or transferred onto a person's skin. To eliminate the possibility of radioactive surface contamination, it is necessary to measure the affected surfaces and areas with an appropriate instrument. [1]

2.3.1 Regulations concerning surface contamination

The Finnish Radiation and Nuclear Safety Authority (STUK) regulates the use of radiation and radioactive materials, and monitors radiation and nuclear safety in Finland. STUK has specific regulations concerning radioactive surface contamination and advises how radioactivity of surfaces should be monitored and how contamination should be contained and cleaned. Table 1 shows limits in surface activity in working areas and equipment, when working in areas where there is a risk of surface contamination.

Table 1. Limits for activity per surface area set by STUK. [5]

Radioactive material	**Working areas and equipment***	
	Control area (Bq/cm^2)	Monitoring area (Bq/cm^2)
Alpha active	4	0,4
Beta active	40	4

*Control area and monitoring area are defined in STUK regulation on operational radiation safety (ST 1.6).

According to Table 1, if there is alpha active contamination on a surface that is considered to be a monitoring area, the maximum activity per surface area should be no more than $0.4\,Bq/cm^2$. If the surface activity is detected to be higher than the limit dictated by STUK, the surface should be appropriately decontaminated, if it can be done safely. STUK requires the activity per surface area to be determined as the average activity measured over a $100\,cm^2$ area. To reliably measure such low levels of alpha activity on a surface as presented in Table 1, one is required use a contamination monitor that is able detect and count individual alpha particles emanating from the surface. [1].

3 Methods and construction

The purpose of this section is to introduce the design and elements that make up the prototype detector, as well as the methods used for achieving the desired properties. Methods for data acquisition are introduced as well. The goal was to build a proof-of-principle prototype of a contamination monitor with positional sensitivity and the ability to detect alpha and beta particles and distinguish between the two. The design of the prototype is largely based on a previous instrument built by Joukainen *et al.*, where a scillator-based detector was built for the detection and measurement of beta particles emanating from the decay of short-lived exotic nuclei produced in fusion-evaporation reactions [13]. The beta detector built by Joukainen achieved positional sensitivity by having strips of scintillator material in two layers in an orthogonal arrangement, that would individually measure the x- and y-coordinates of a high energy beta particle passing through both layers. As the prototype that was built for this thesis work had to be able to also detect alpha particles, which would not penetrate two layers of scintillator plastic, a different approach for positional sensitivity was needed. Also, a method for separately detecting said alpha particles was needed.

3.1 Data acquisition

Data collection was performed with a 16-channel Lyrtech/Nutaq VHS-ADC board, with a sampling rate of 105 MHz. Two channels were used to collect traces from two silicon photomultipliers that were coupled to a single bar of plastic scintillator. The measurement data was brought into Grain – a data analysis software developed for nuclear spectroscopy experiments [14]. The data was analyzed with a Java-written script, which utilized pulse shape discrimination to separately measure fast and slow signals (described in Section 3.3), and signal attenuation to evaluate the position of the incoming particles (described in Section 3.2).

3.2 Positional sensitivity

The approach for achieving positional sensitivity was based on the controlled attenuation of light. Previous experiments conducted by Joukainen *et al.* showed that coating an oblong bar of scintillator plastic with white paint resulted in the attenuation of the light signal along the length of the bar. Presumably the diffusive reflections and partial absorptions in the white paint made the measured signal strength dependent on the distance traveled in the plastic scintillator before detection.

In this work, an experimental setup was constructed where two SiPMs were optically coupled to the ends of a 10 cm long bar of plastic scintillator, made of polyvinyl toluene (PVT) doped with anthracene (Saint-Gobain BC-412). The plastic scintillator coated in white paint (Eljen Technologies EJ-510 Reflective Paint). The choice of materials was based on the previous experimentation conducted by Joukainen and the need to investigate the reported positional sensitivity further [13].

An experiment was conducted, where a collimated alpha source of ^{241}Am was perpendicularly pointed towards the bar of PVT in such a way, that the tip of the collimator was at a 2 mm distance from the surface of the bar. The alpha source was moved in 5 mm increments along the length of the bar for each measurement. Signal intensities from each event were measured from both ends of the bar for 2 minutes at each position. The experiment setup is illustrated in Figure 13.

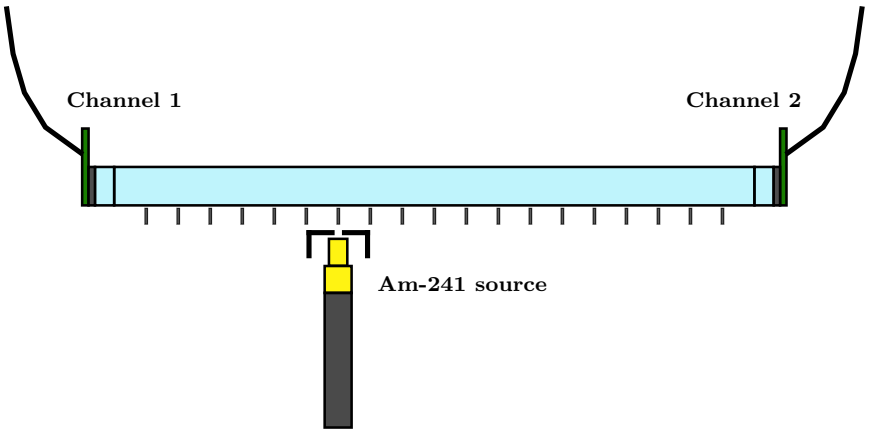

Figure 13. The collimated ^{241}Am alpha source was pointed towards the 10 cm long scintillator bar, which was coated in white paint. The source was moved along the length of the bar at 5 mm increments, while it was kept at a 2 mm distance. Each tick is a 5 mm increment.

As the radiation source was moved along the length of the bar, the signal intensities measured from the two channels would change according to the position of the event. Figure 14 shows the change in signal intensity when the radiation source was moved further from one SiPM and closer towards the other.

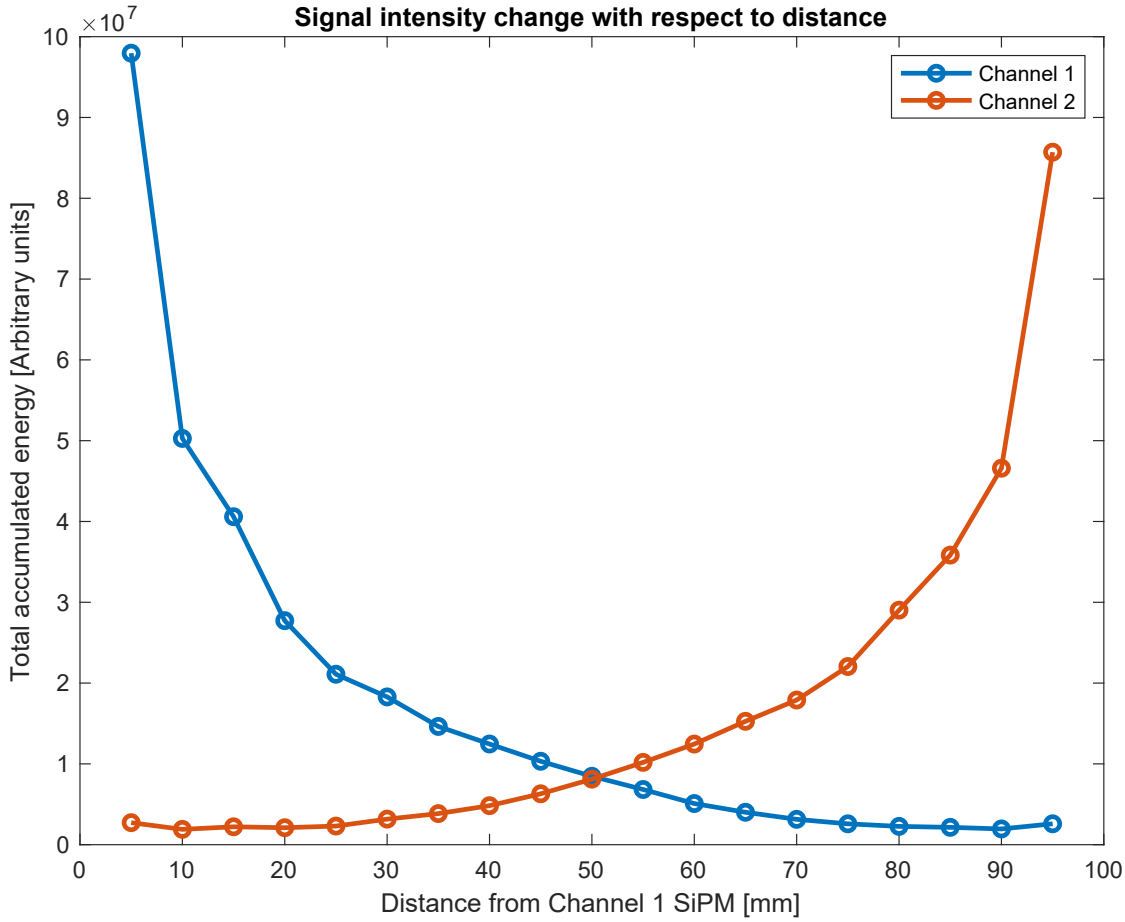

Figure 14. Signal strength change as a function of distance. The signal strength decreases as the radiation source is moved further away from the silicon photomultiplier and the light from the scintillation has to travel a longer distance in the plastic. Conversely, the signal strength increases in the opposite channel as the source is moved closer to it. Channel 1 SiPM is at position 0 mm, and channel 2 SiPM is at position 100 mm.

As demonstrated by Figure 14, the signal intensities I_{Ch1} and I_{Ch2} from channels 1 and 2, are functions of position x along the length of the bar. This means that the the signal intensities can be used to obtain information about the position. The ratio

$$R(x) = \frac{I_{\mathrm{Ch1}}(x)}{I_{\mathrm{Ch1}}(x) + I_{\mathrm{Ch2}}(x)}. \tag{13}$$

would then be a function of the position as well. Ideally, for each event occurring in a specific position along the length of the bar, there would be a corresponding ratio R. For example, if the scintillation event would occur exactly halfway between the two ends, ideally R would be equal to 0.5, since both signals contribute equally.

In actuality, a distribution of R is measured at each position. Figure 15 shows distributions of R from multiple measurements measured at 15 mm increments along the length of the bar. For clearer demonstration, not every measurement with 5 mm increments is presented in the figure.

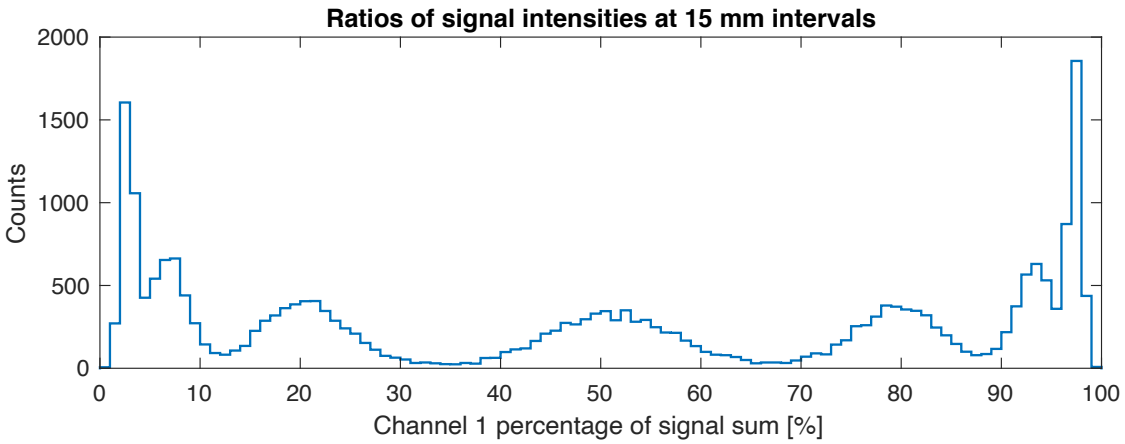

Figure 15. Distributions of R from events measured 5, 20, 35, 50, 65, 80 and 95 mm positions for 2 minutes. Each peak position on the x-axis corresponds to a longitudinal position in the scintillator bar in between the SiPMs.

The data in Figure 15 can be used as calibration data, so that a ratio R could be transformed into a value that would represent a real position in between the SiPMs. The calibration was done by taking the mean of each distribution and using that as the x-data, taking corresponding position from each measurement as the y-data, and fitting a curvilinear function to the data. The function obtained from the fit is

$$\mathrm{P}(R) = \left(\frac{R}{49.63}\right)^{0.1722}, \tag{14}$$

which would now project any measured R into a real position along the length of the bar. The calibration function would lose its accuracy if $I_{\mathrm{Ch2}}(x) > I_{\mathrm{Ch1}}(x)$, so in that case, the input to the function should be $(1 - R)$ instead of R. When the data in Figure 15 is fed into Equation (14), it is transformed into the real positions where the radiation source was placed during measurement. The transformed data showing the positions is shown in Figure 16.

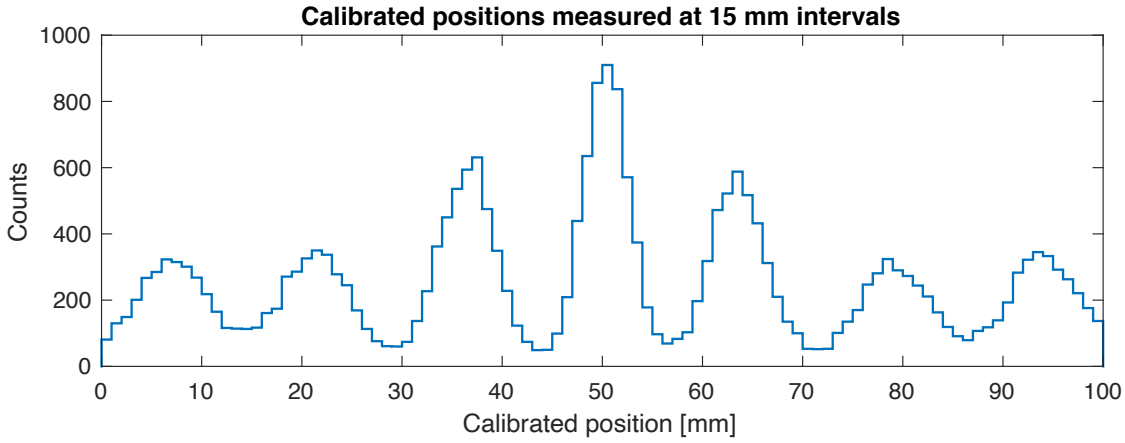

Figure 16. The distributions of R from Figure 15 transformed into into positions through the calibration function in Equation (14). The peaks are now approximately at the 5, 20, 35, 50, 65, 80 and 95 mm positions, as they should be.

Figure 16 shows that the calibration was succesful, and that measured signals and the ratio of their intensities can be converted into real positions along the length of the scintillator bar.

3.3 Alpha/beta discrimination

The approach used to distinguish between alpha and beta radiation is based on the method of *pulse shape discrimination*, which relies on the two types of radiation producing signals that differ in shape from one another. Any type of radiation hitting a piece of scintillating material produces a signal whose pulse height is dependent on the energy transferred in the event, and whose shape is dependent on the fluorescent properties of the scintillator. Since alpha and beta particles hitting the same piece of scintillating material would produce two similar signals, different scintillating materials are needed to separately detect them.

Polyvinyl toluene (PVT) is an optically transparent organic polymer which, when doped with anthracene, makes a plastic scintillator. When bombarded with energetic particles, a plastic PVT scintillator produces a signal with a fast rise time and a fast decay time, with a pulse duration of 500 ns – 1000 ns. Zinc sulphide, when doped with silver, makes another type of scintillator which produces a signal that is significantly slower in rise and decay times when compared to PVT. Zinc sulphide exists mainly in white powder form, but can be synthetically made in to an optically clear crystalline form.

Figure 17 illustrates how a layer of ZnS on top of a piece of PVT scintillator can cause the two types of radiations to induce scintillation separately in the two materials.

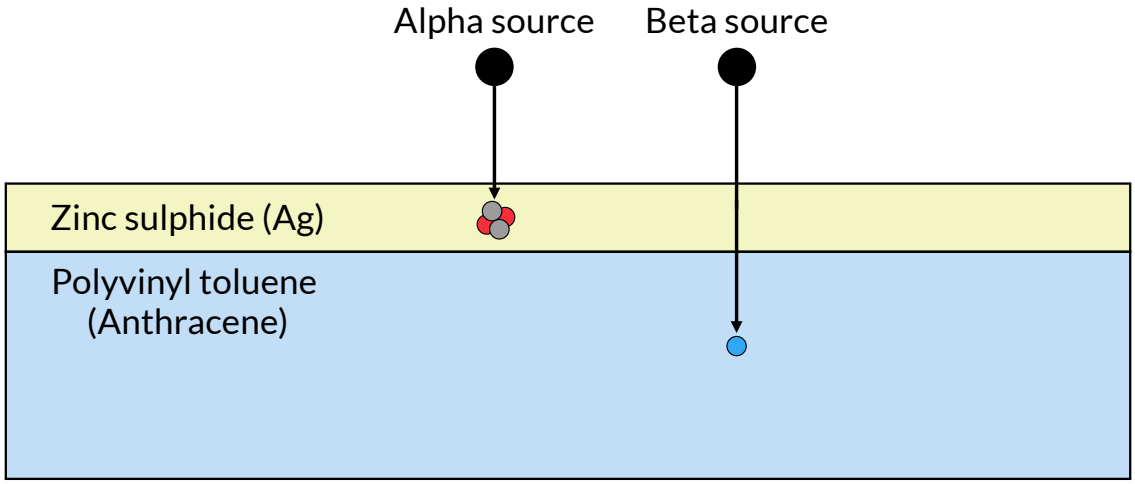

Figure 17. Alpha particles and beta particles penetrating material. Alpha particles are stopped in the ZnS and cause it to scintillate. Fast electrons penetrate deep enough to cause scintillation in the plastic.

As we irradiate a piece of PVT that has been layered with ZnS, the resulting pulses of light are detected by the silicon photomultipliers coupled to the plastic, which convert the light pulses into electrical signals. As the electrical signals are then recorded with our digital data collection system, we get two distinct signal shapes, depending on the type of radiation is used. The signal shape recorded when an alpha source was used for irradiation is shown in the upper graph of Figure 18. The lower graph in Figure 18 represents the signal that is recorded when the scintillator is irradiated with a beta source.

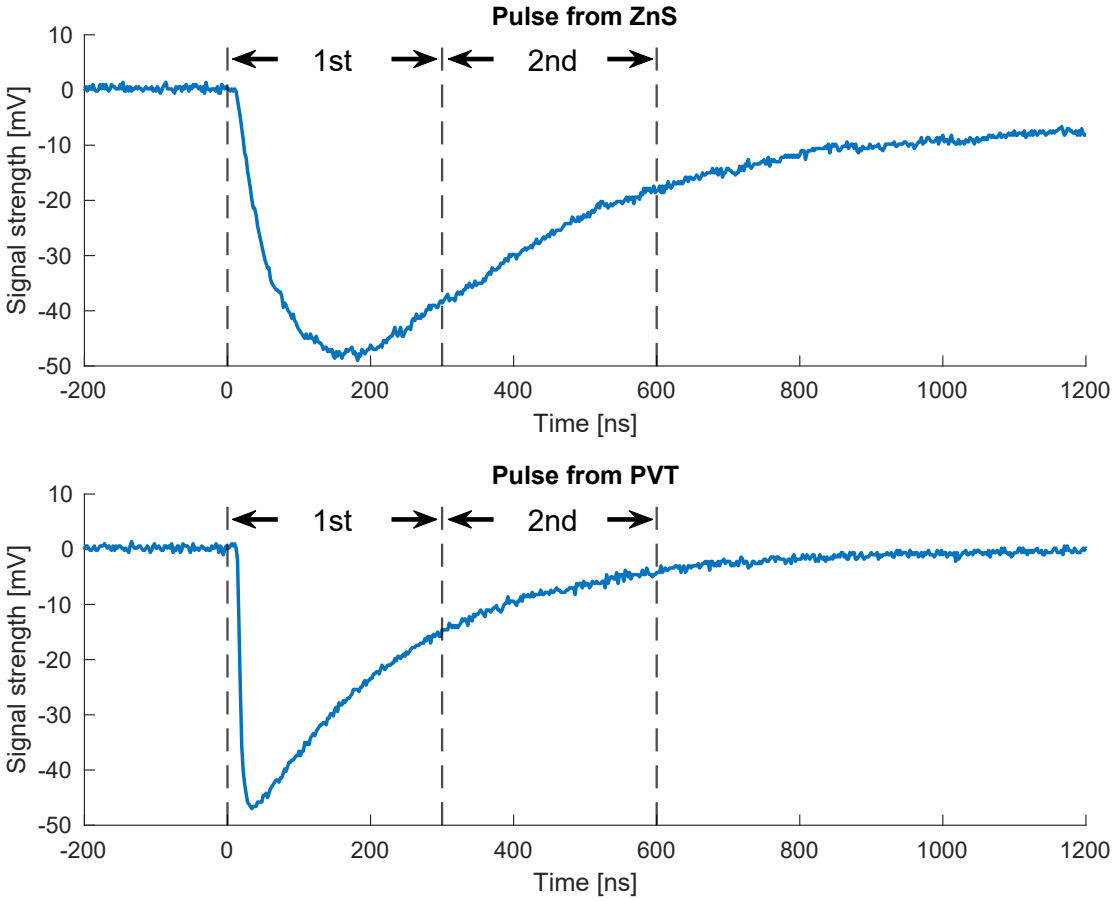

Figure 18. Pulse shapes from scintillation events produced in ZnS (above) and PVT (below). The slower signal in ZnS is produced by alphas hitting the ZnS layer on top of the PVT, while the faster signal is produced by betas penetrating into the plastic. The dashed lines represent limits for partial integrations used in pulse shape discrimination.

These two kinds of signals can be distinguished from one another by analyzing the pulse shapes. The pulse shapes can be analyzed by taking two partial integrations

(*i.e.* sums of the signal values) over both pulses with the same integration limits. The partial integration limits are represented by the dashed lines in Figure 18. Because of the shape and the duration of the ZnS pulse, the ratio between the partial integrations (1st/2nd) is smaller when compared the same value obtained from the sharp PVT signal. These two different values can be plotted into a 2D histogram, which is shown in Figure 19.

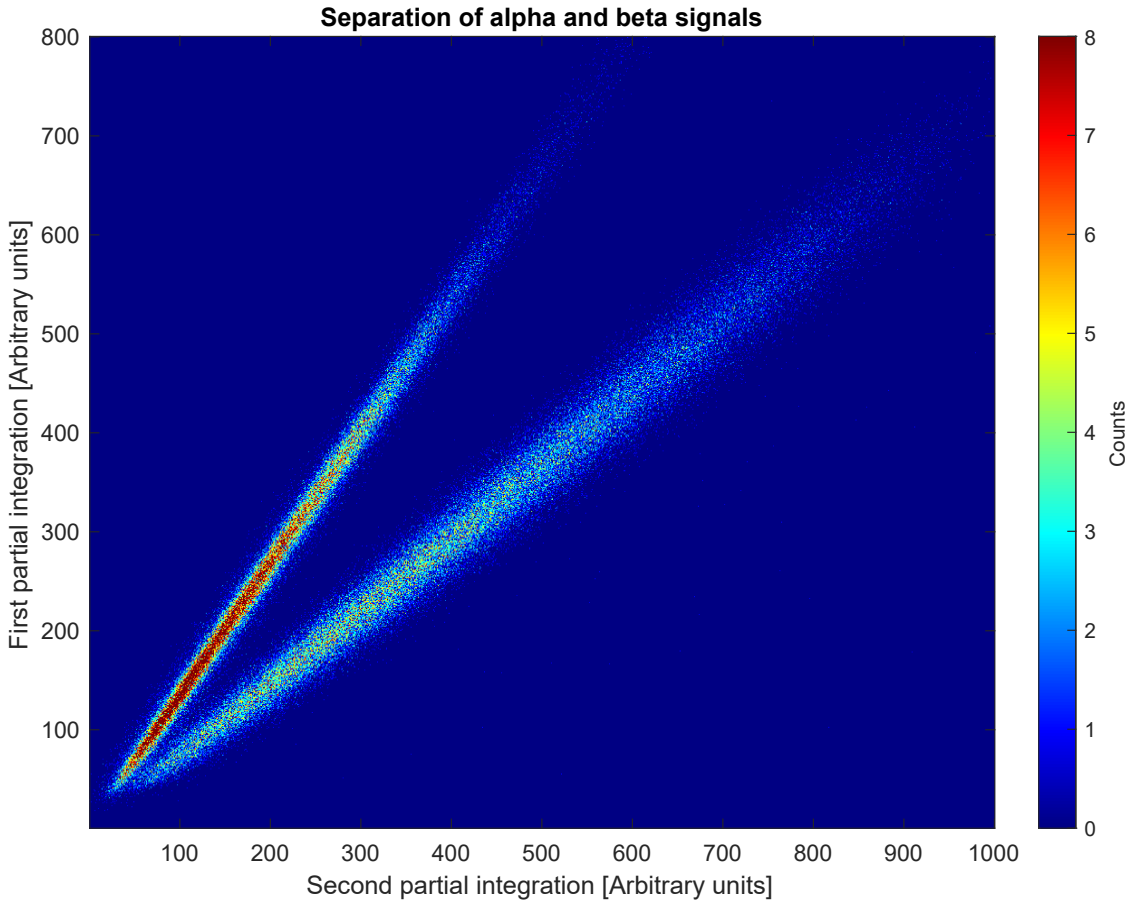

Figure 19. The partial integrations of both ZnS and PVT signals plotted in a 2D histogram. The streak with a steeper slope represents the fast signals measured from the PVT, while the gentle slope represents the signals measured from ZnS.

Because the ratio of partial integrations over the two different pulse shapes results in two distinct values, it can be used as a criterion by which the signals are sorted into alpha particles or beta particles. This method of pulse shape discrimination allows for the separate detection of alpha radiation and beta radiation.

3.4 Manufacture and assembly

After methods for positional sensitivity and separation of alpha and beta radiations had been established, it was time to scale up the model and build a full working prototype. The plastic scintillator used was polyvinyltoluene doped with anthracene (Saint-Gobain BC-412), a hydrocarbon which consists of three benzene rings fused together. The bars were initially cut from a large block of bulk PVT scintillator, and then machined in to the desired dimensions of 6 mm × 10 mm × 100 mm with a milling machine. The light guides were manufactured in a similar manner, first cut from a slab of poly(methyl methacrylate) (Plexiglas®) and then machined into the desired dimensions. The surfaces of the bars and light guides were sanded and polished by hand to make them as optically clear as possible. The light guides were coupled to the ends of the scintillator bars with an optically clear epoxy (Araldite®), whose refractive index was 1.553, the same as that of glass. A single scintillator bar with the light guides attached is shown in Figure 20.

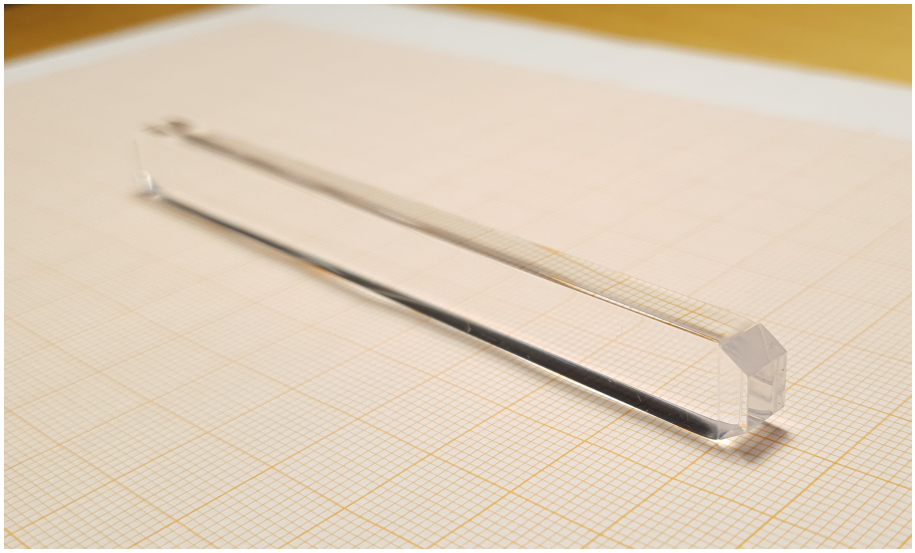

Figure 20. Bar of scintillator plastic with acrylic light guides attached to the ends.

Ten bars, such as the one shown in Figure 20 were manufactured, as shown in Figure 21. The scintillator bars were subsequently coated with white paint for the purpose of positional sensitivity, as explained in Section 3.2. The paint used was regular white acrylic primer from a spray can, because it was shown to work just as well as EJ-510 Reflective Paint, but it resulted in a more even coat and the

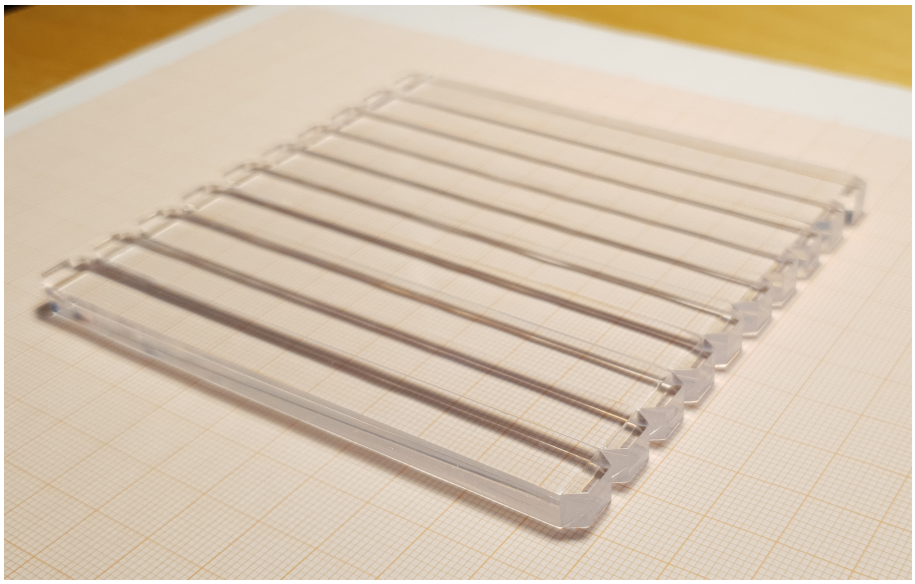

Figure 21. An array of ten scintillator bars that would later become the 10 cm × 10 cm face of the detector.

application was faster and easier. The only areas left uncoated were the ends, to which the SiPMs were to be coupled, and one of the 10 mm × 100 mm sides, onto which the layer of ZnS(Ag) was to be applied. A single paint coated bar is shown in Figure 22.

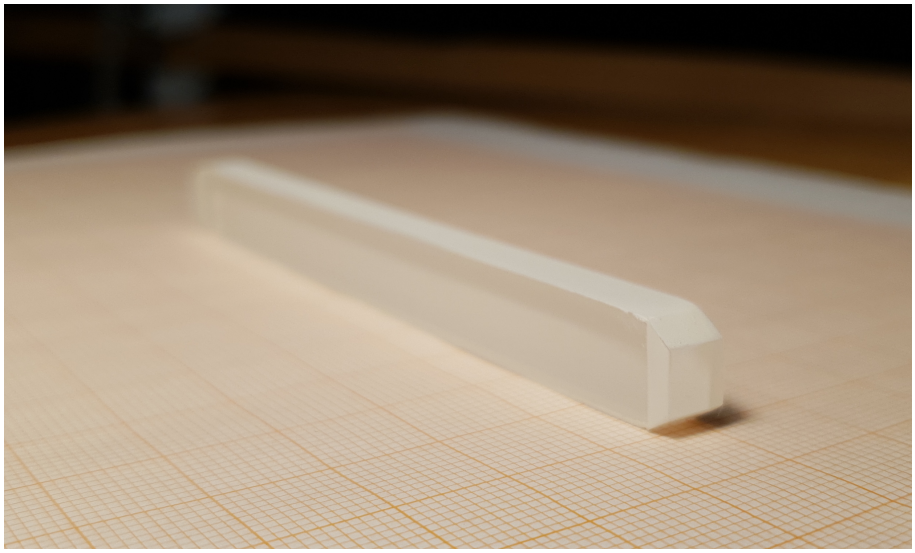

Figure 22. A scintillator bar coated in white paint, except for the ends and one of the faces.

Once all of the bars were painted, the exposed 10 mm × 100 mm faces were fully

covered with sheets of ZnS (Ag), for the purpose of separately detecting alpha and beta radiation, as explained in Section 3.3. A generous amount of optical couplant was squeezed in between to ensure that light yielded in the ZnS would travel through and into the transparent plastic. After attaching the layers of ZnS, the bars were then wrapped in 5 µm thin aluminized mylar foil, to help isolate them from any light yielded in an adjacent bars. The mylar foil was tested to be thin enough for alpha particles to pass through, but thick enough to provide sufficient light isolation. A bar that has been wrapped in mylar is shown in Figure 23.

Figure 23. A bar of scintillator plastic coated in white paint, with a layer of ZnS on top, fully wrapped in mylar. This is a fully finished scintillator element ready to be used in the finished prototype.

Once all ten of the bars were taken through these aforementioned steps, they were finished scintillator elements ready to be used in the detector. Structural parts for the prototype were designed in a CAD software and 3D printed using PLA (polylactic acid) filament. The scintillator elements were placed side by side and the array was mechanically held together by some screws and the 3D printed parts. The assembled detector face is shown in Figure 24. Once the face of the detector was assembled, arrays of photomultipliers were coupled to both ends of the scintillator elements. An array of silicon photomultipliers is shown in Figure 25.

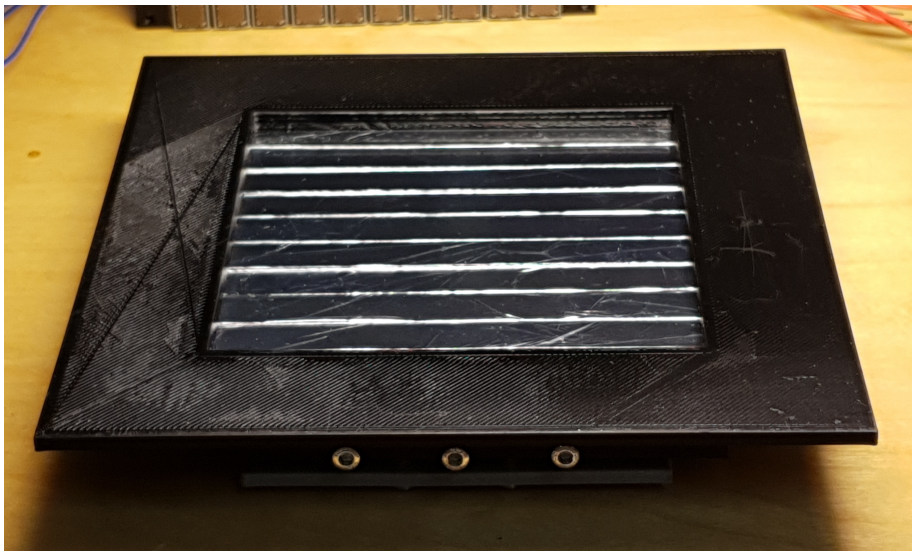

(a)

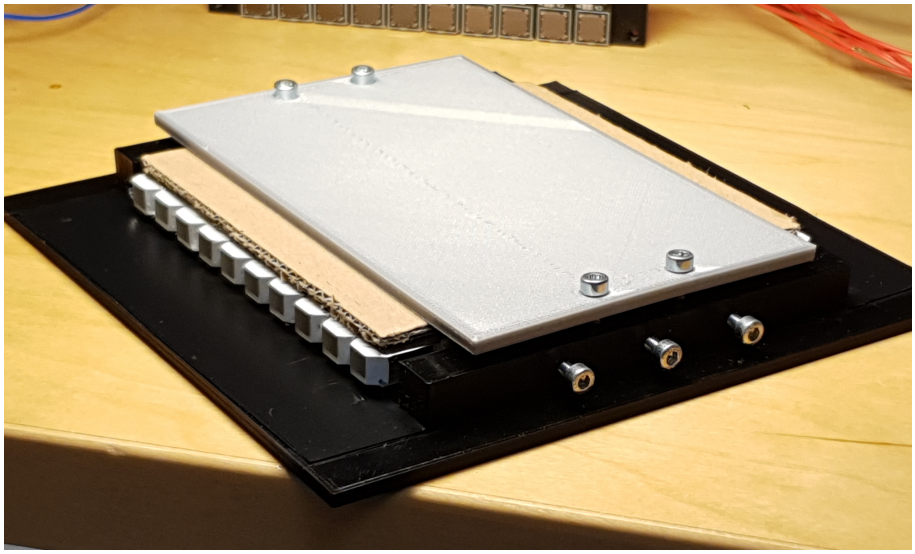

(b)

Figure 24. (a) The face of the detector. The finished scintillator elements are seen side by side. **(b)** The backside of the assembled detector. The exposed ends of the scintillator elements are seen protruding from the structure. This is where the silicon photomultipliers would later be coupled.

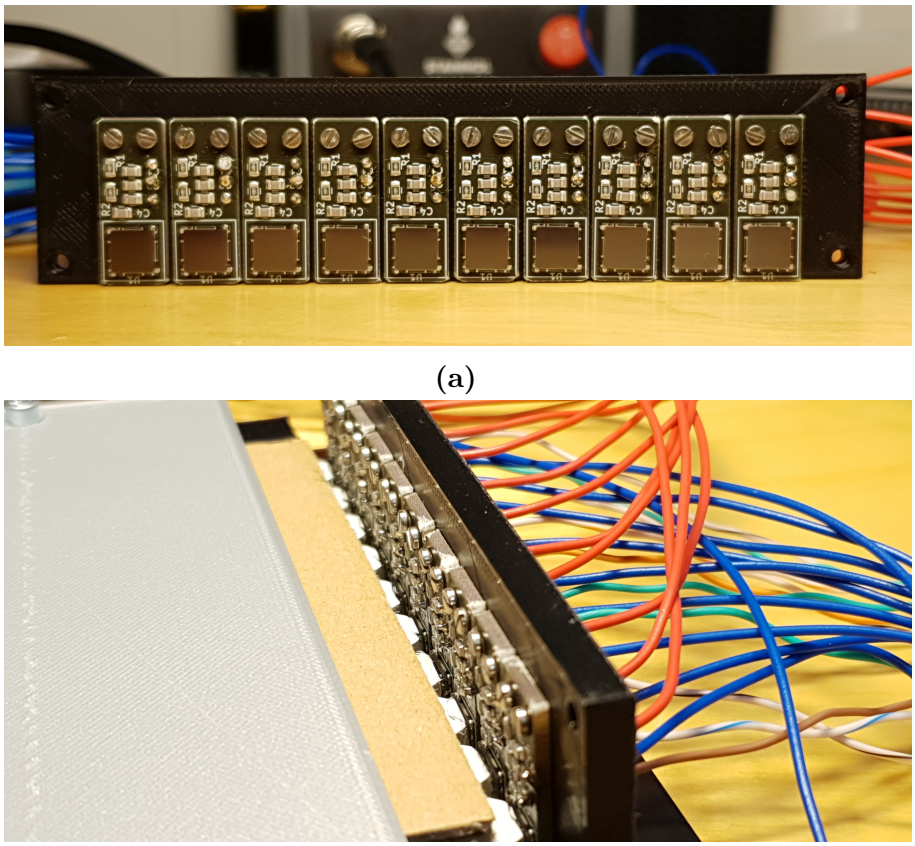

(a)

(b)

Figure 25. (a) An array silicon photomultipliers screwed onto a 3D printed holder. **(b)** The same array coupled to the scintillator elements with optically transparent grease.

After coupling the photomultipliers to the scintillator elements, cables for the bias voltage required for operation were soldered onto the chips, as well as coaxial cables for signal measurement. The apparatus was then placed in a plastic box, so that measurements could be performed in total darkness. The box can be seen in Figure 26 and the measurements are presented in Section 4. The appropriate cable inlets were drilled into the box walls, so that the system had twenty coaxial LEMO-outputs for data collection, as well as a single coaxial LEMO-input for applying the bias voltage to all of the silicon photomultipliers.

4 Measurements

4.1 Collection of measurement data

The data collection was performed in the same way as was presented in Section 3.1. Only this time *two* 16-channel Lyrtech/Nutaq VHS-ADC boards were used with their clocks synchronized. Twenty of the 32 available channels were used to collect data from the twenty photomultipliers that were coupled to plastic scintillator elements in the detector.

4.2 Testing discrimination and positional accuracy

In preparation for the measurements, an acrylic plate with collimator holes drilled into measured positions was manufactured. The collimator holes were designed to suspend radiation sources above the face of the detector, to simulate a situation where the prototype would be used to detect a point source contamination on a surface.

An ^{241}Am source was placed in the center hole of the collimator plate and a ^{90}Sr source was placed in the bottom right corner hole. A function in the Java sort script was used to separate fast signals from slow signal by means of pulse shape discrimination, as described in Section 3.3. The measurement setup can be seen in Figure 26. Data was gathered for a total of 1 minute.

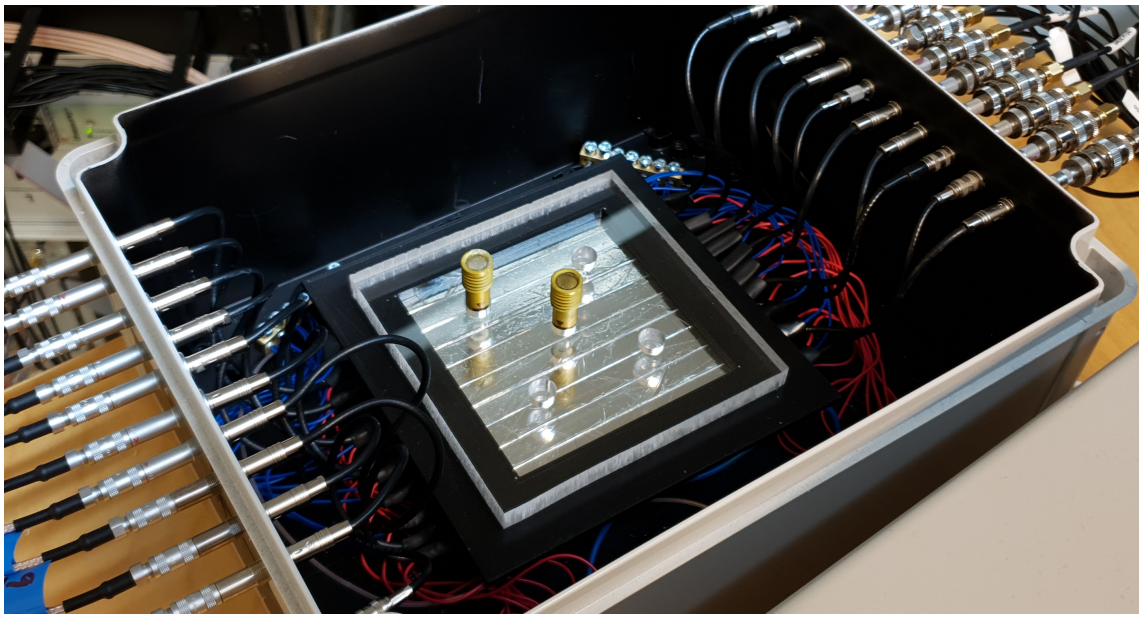

Figure 26. The measurement setup showing alpha (middle) and beta (corner) radiation sources pointing towards the detector face.

The measurement arrangement presented in Figure 26 yielded the data that are shown in Figures 27a, 27b and 28. These figures represent a map of the face of the detector, essentially a coordinate system, where the x-axis represents the position of an event within a single scintillator bar, and the y-axis represents which bar the event occurs in. Figure 27a depicts events that produce slow signals and, as can be seen, only shows signals measured at the center of the detector where, in this particular measurement, the alpha source is suspended. Figure 27b respectively shows events that produce fast signals, which are measured at the lower right corner of the detector, where the beta source was suspended. These figures display the simultaneously detected two types of radiation separately, while also providing the information regarding the position of their sources.

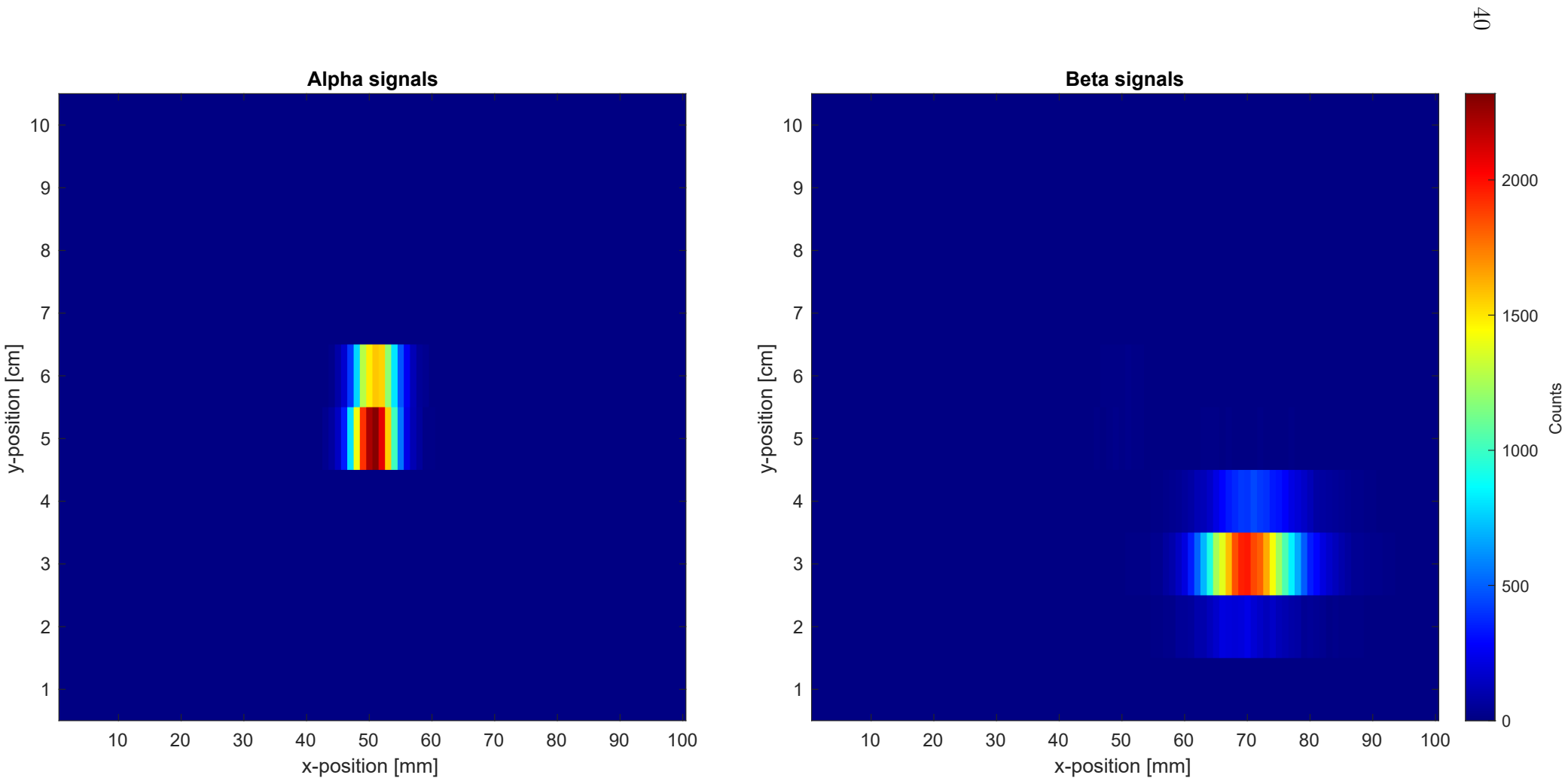

(a) **(b)**

Figure 27. Two dimensional histograms presenting data from a measurement where an alpha source was suspended over the center of the detector and a beta source was suspended over the lower right corner. The events were gathered into different histograms by means of pulse shape discrimination. **(a)** displays slow signals produced by alpha particles and **(b)** displays fast signals produced by betas. Both figures show the respective computed positions of the radiation sources.

Figure 27b also shows a small amount of fast signal coming from the center of the detector as well. This is caused by alpha particles passing through the gaps in between the ZnS sheets and reaching the PVT and producing false beta signals. Figures Figures 27a and 27b can be combined (Figure 28), to show the complete positional map of all radiation detected.

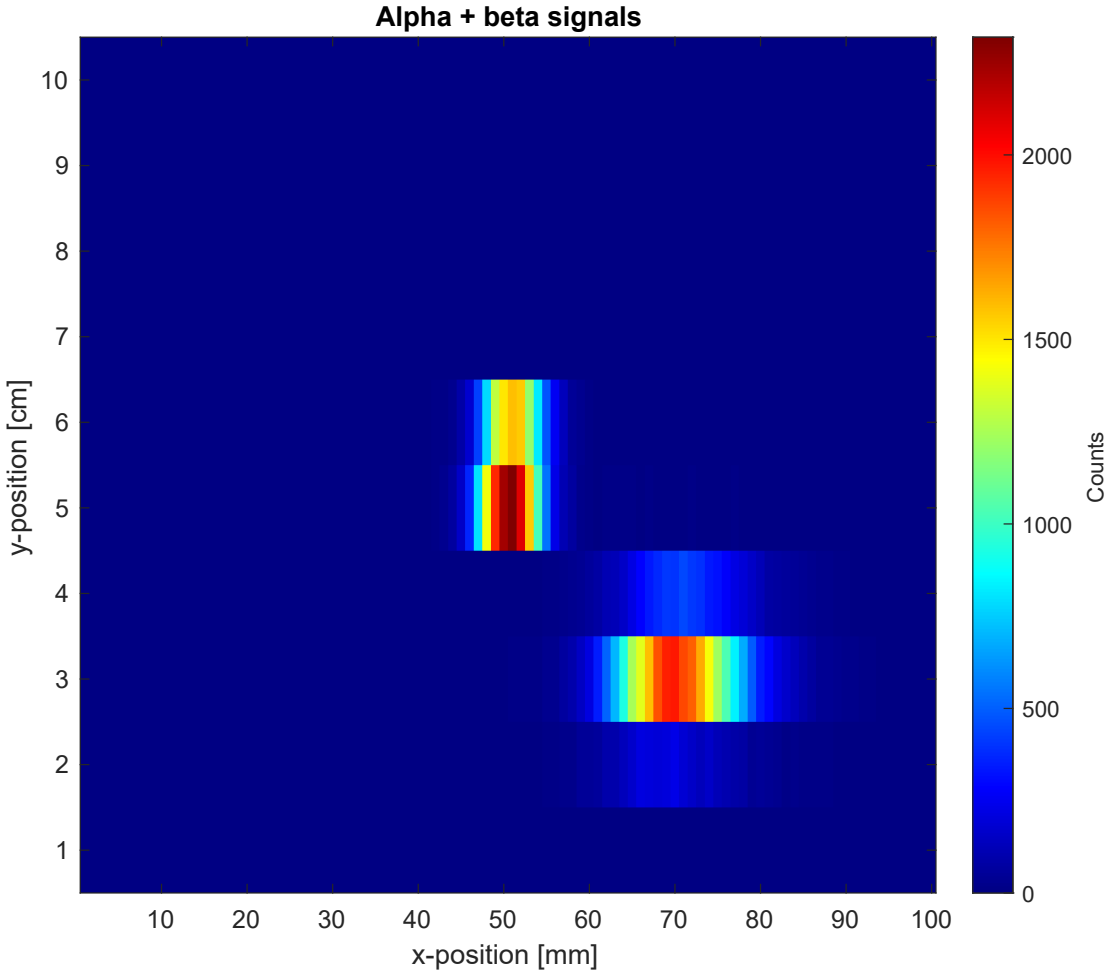

Figure 28. A 2D histogram showing the combined data from figures Figures 27a and 27b. It shows the positional information of all radiation detected.

The true position of the suspended alpa source was the center of the $10\,\mathrm{cm} \times 10\,\mathrm{cm}^2$ detector, pointing directly in between bars 5 and 6. Its position in the detector surface's coordinate system was thus $p_\alpha = (5\,\mathrm{cm}, 5\,\mathrm{cm})$. The beta source was suspended at $p_\beta = (7.375\,\mathrm{cm}, 2.625\,\mathrm{cm})$. The positions can also be calculated according to the measured data. One can analyze the positional accuracy of the detector in the x-direction by taking the full width at half maximum of a signal. For the distribution

of alpha signals in bar 5 and 6, the x-position was measured to be $50 \pm 4\,\text{mm}$. The position was taken to be the center of the distribution, and the uncertainty was taken to be half of the full width at half maximum. If we analyze the relationship of the intensities between bars 5 and 6, get that the the signal was divided between the two approximately 60% to 40%. It is not possible to calculate exactly the y-position of the alpha source, but one could deduce that it was approximately in between the bars 5 and 6. For the distribution of beta signals in bar 3 the x-position was similarly measured to be $69 \pm 6\,\text{mm}$. The beta signals have a wider spread due to scattering and the varying ranges of the distribution of beta particles across different energies.

4.3 Testing gamma ray transparency

The sensitivity for detecting gamma rays was also tested for the detector. A ^{60}Co source of approximately 1.25 MBq was placed on top of the lid of the box which contained the detector, along with an alpha source once again suspended over the center, and a beta source over the lower left corner of the detector surface. The source information and the setup can be seen in Figure 29. Data was gathered for a total of one minute.

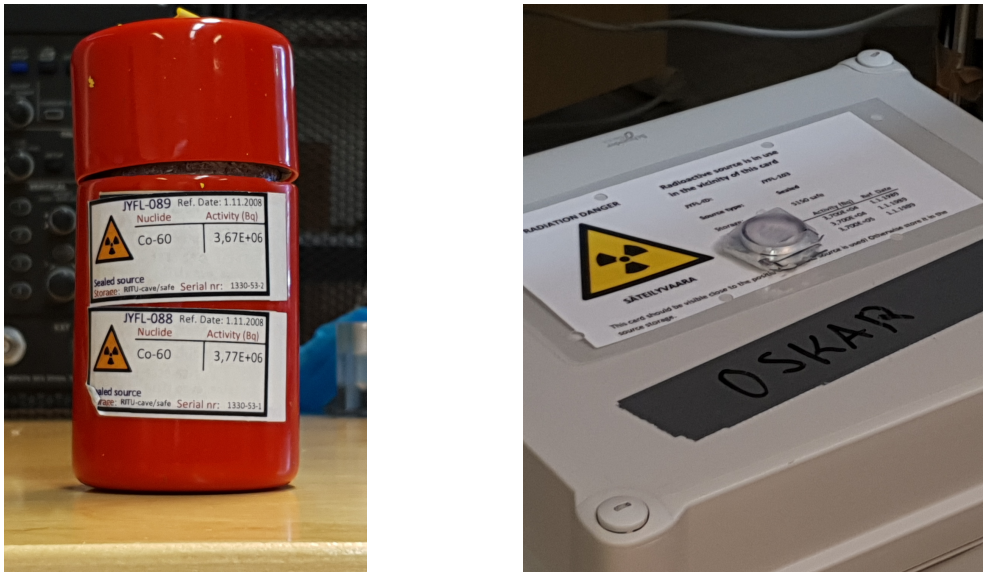

(a) **(b)**

Figure 29. **(a)** shows the gamma source used for the measurement. The label shows the measured activity on the reference date, but on the date of measurement the remaining activity was calculated to be 1.25 MBq. **(b)** shows the placement of the gamma source on top of the box that contained the detector.

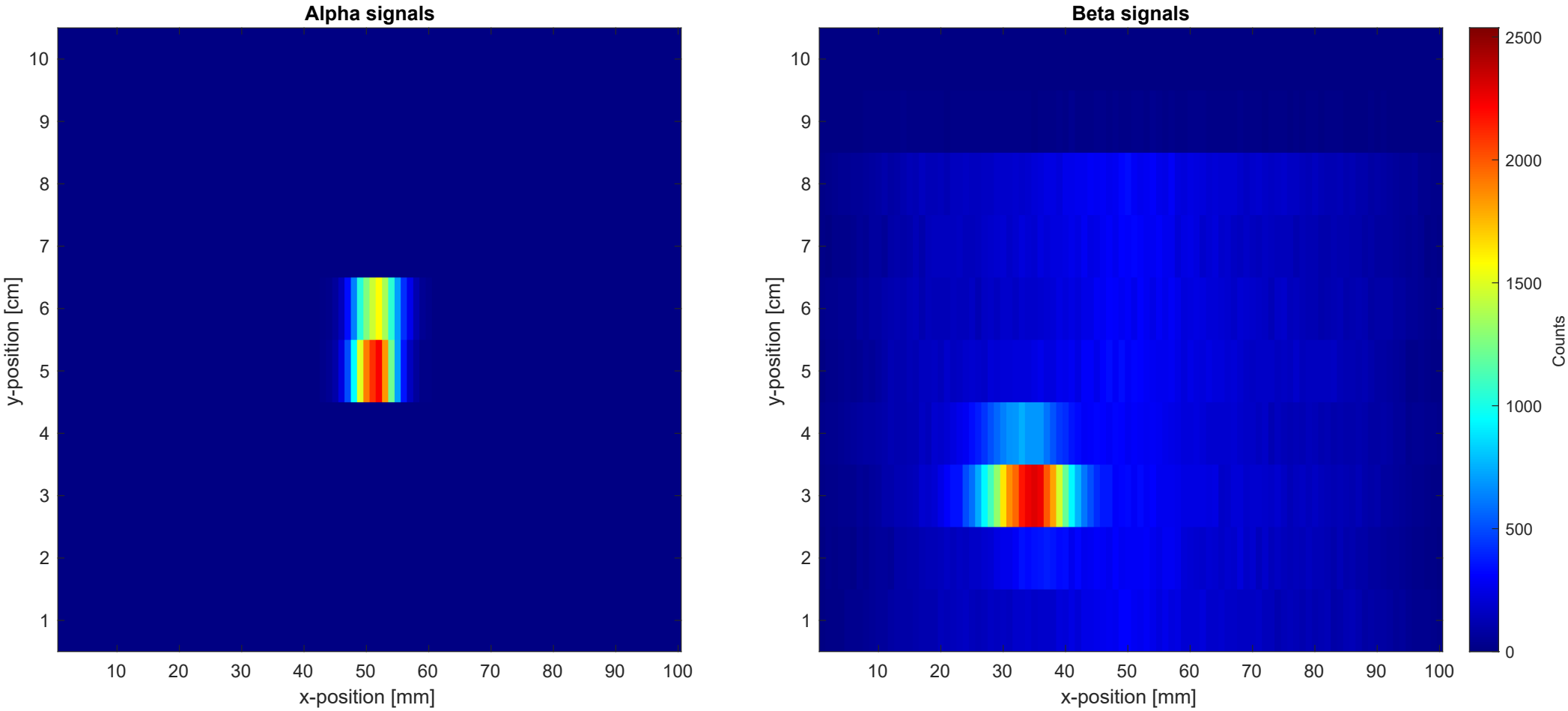

(a) **(b)**

Figure 30. Histograms presenting data from a measurement where an alpha source was suspended over the center of the detector, a beta source was suspended over the lower left corner and a gamma source was placed over box containing the system. **(a)** shows the slow signals produced by alphas, while **(b)** shows the fast signals, caused by betas, as well as an increased background caused by gamma rays interacting in the PTV scintillator.

Figure 30 shows the results of the gamma experiment. One can see that the gamma source placed on top increased the background level of the fast signal map. This is presumably because the 1173.2 MeV and 1332.5 MeV gamma rays are unlikely to interact in the thin layer of zinc sulphide, and more likely to be attenuated in the PVT scintillator and produce a signal there. Essentially gamma rays that interact in the PVT are interpreted as betas, since the signals they produce are indistinguishable from one another. Figure 31 once again shows the combined 2D map from the gamma experiment, showing both the fast and slow signals in one figure.

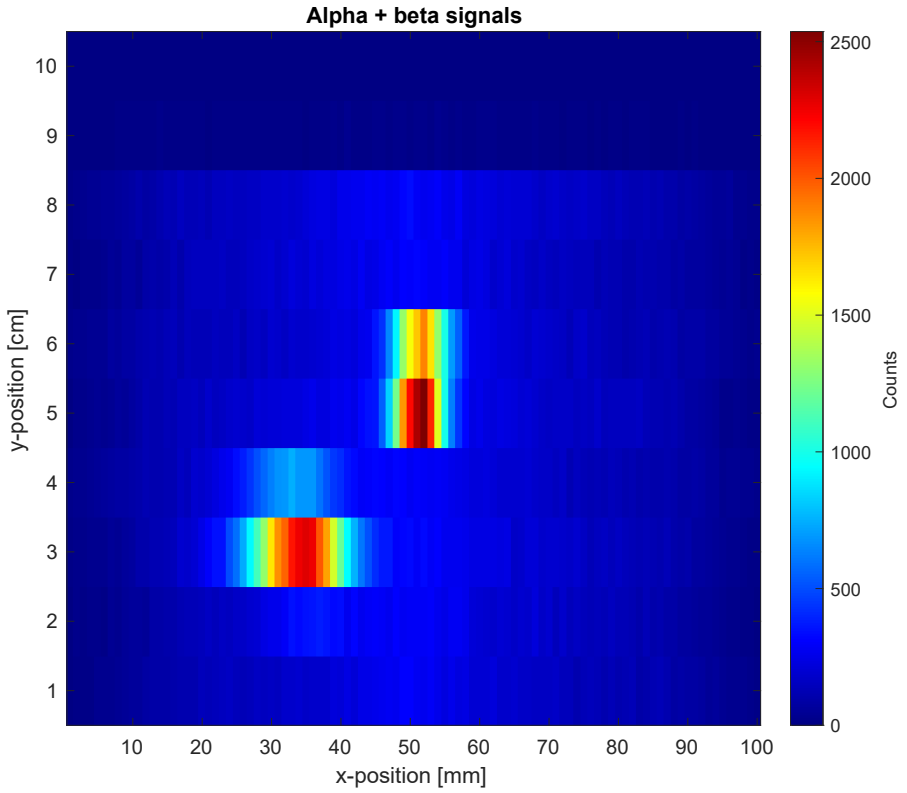

Figure 31. Signals form alpha radiation (center), beta radiation (lower left corner), and gamma radiation (background) all in one heatmap. The signals from bars 9 and 10 are not abundant, because the data channels were defective.

5 Conclusions

The goal of this work was to build and test a proof-of-principle prototype of a surface contamination monitor, which would have the ability of detecting alpha radiation and beta radiation separately, all the while measuring the positions of the radiation sources. The motivation behind this goal was to advance and combine the techniques used for alpha/beta discrimination and positional sensitivity, so that they could potentially be used in the construction of a more ideal contamination monitor, that would include but would not be limited to these properties.

The method of putting zinc sulphide on top of the PVT scintillator, and using pulse shape discrimination to tell discriminate alpha and beta radiation worked to a satisfactory degree. The only exception was when alpha particles managed to hit gaps in between zinc sulphide sheets and hit the PVT scintillator directly, they produced false beta signals. This effect was very minimal and could be avoided with a different design, where the whole detector surface was covered in a single ZnS sheet, rather than each PVT bar having their own sheet, with gaps in between. But essentially, during experimentation when an alpha source and/or a beta source was placed over the detector, the signals would appear in separate maps, showed that the separate detection of the two types of radiation was succesful.

Using white paint to coat the scintillator plastic in order to attenuate light and thus make the strength of the scintillation signal positionally sensitive, was also succesful but with certain shortcomings. The measured positional accuracy for alpha particles was approximately 8 mm along the length of the oblong scintillator bar. The accuracy for beta particles was measured to be approximately 12 mm, which is not as accurate due to the scattering of electrons. The accuracy in the perpendicular direction is discretely 1 cm, because the bars were one centimeter wide, but when a single point source is placed in roughly in between two scintillator bars, this introduces some uncertainty to the y-position of the source. One would have to measure how the signal intensities change when a source is moved from the middle of one bar, over the gap to the middle of the adjacent bar, which was not done in this work. Overall

the positional resolution achieved was roughly 1 cm, although it was not tested how the energy of the radiation would affect the positional accuracy.

In conclusion, the objectives that were set for this project were essentially met. A prototype was built with the desired properties of alpha/beta discrimination and positional sensitivity. The evidently succesful methods utilized to achieve these properties can then in the future be applied when building a radiation detector that requires similar functionality.

If one wanted to implement nuclide identification with this design, one would have to use a thick layer of scintillator material that was dense enough to attenuate gamma rays, and had a good energy resolution. This would have to be yet another separate layer of scintillator, which would produce a third kind of pulse shape distinguishable from the pulse shapes produced by the PTV and ZnS. An alternative would be to use semoconductor-based solution for gamma ray detection and energy measurement.

References

[1] H. Tuovinen, *Kontaminaation mittaus säteilyn käytössä.* STUK, Teollisuuden ja tutkimuksen 12. säteilyturvallisuuspäivät, 2017.

[2] W. Paile, "Säteilyn terveysvaikutukset. 2002," *Part of the Säteily-ja ydinturvallisuus book series published by STUK. In Finnish.*

[3] G. F. Knoll, *Radiation Detection and Measurement.* John Wiley & Sons, 2010.

[4] K. S. Krane, *Introductory Nuclear Physics.* John Wiley & Sons, 1991.

[5] P. Piippana and T. Toivonen, *Määräys, STUK S/1/2018: Säteilyturvakeskuksen määräys työperäisen altistuksen selvittämisestä, arvioinnista ja seurannasta.* STUK, 2018.

[6] R. D. Evans and R. Evans, *The Atomic Nucleus*, vol. 582. McGraw-Hill New York, 1955.

[7] C. A. Kelsey, P. H. Heintz, G. D. Chambers, D. J. Sandoval, N. L. Adolphi, and K. S. Paffett, *Radiation Biology of Medical Imaging.* John Wiley & Sons Incorporated, 2014.

[8] F. M. Khan and J. P. Gibbons, *Khan's The Physics of Radiation Therapy.* Lippincott Williams & Wilkins, 2014.

[9] International Atomic Energy Agency Nuclear Data Services. Nuclear Structure and Decay Data. URL: `https://www-nds.iaea.org/relnsd/vcharthtml/VChartHTML.html`.

[10] Released into the public domain by the copyright owner Inductiveload. URL: `https://commons.wikimedia.org/w/index.php?curid=2858666`.

[11] M. Lowdon, P. G. Martin, M. W. Hubbard, M. P. Taggart, D. T. Connor, Y. Verbelen, P. Sellin, and T. B. Scott, "Evaluation of scintillator detection materials for application within airborne environmental radiation monitoring," *Sensors*, vol. 19, no. 18, p. 3828, 2019.

[12] Image by Qwerty123uiop, license CC BY-SA 3.0, URL: https://commons.wikimedia.org/wiki/File:PhotoMultiplierTubeAndScintillator3.pdf.

[13] H. Joukainen, J. Sarén, and P. Ruotsalainen, "Position sensitive plastic scintillator for beta particle detection," *Nuclear Instruments and Methods in Physics Research Section A: Accelerators, Spectrometers, Detectors and Associated Equipment*, p. 166253, 2021.

[14] P. Rahkila. Grain - A Java Data Analysis System for Total Data Readout. URL: http://users.jyu.fi/~pajura/grain/rahkila-grain-nim.pdf.